# Structural Premise of Selective Deubiquitinase USP30 Inhibition by Small-Molecule Benzosulfonamides

Darragh P O'Brien[1*], Hannah BL Jones[1], Franziska Guenther[2], Emma J Murphy[2], Katherine S England[2], Adán Pinto-Fernández[1,3], Malcolm Anderson[4], Paul Brennan[2], John B Davis[2], Andrew P Turnbull[5], and Benedikt M Kessler[1,3*]

[1]Target Discovery Institute, Centre for Medicines Discovery, Nuffield Department of Medicine, University of Oxford, UK

[2]ARUK-Oxford Drug Discovery Institute, Centre for Medicines Discovery, Nuffield Department of Medicine, University of Oxford, UK

[3]Chinese Academy of Medical Sciences Oxford Institute, University of Oxford, UK

[4]Waters Corporation, Wilmslow, Cheshire, UK

[5]Cancer Research Horizons, Francis Crick Institute, London, UK

*Corresponding authors: darragh.obrien@ndm.ox.ac.uk; benedikt.kessler@ndm.ox.ac.uk

Running Title:

Exploring the molecular and structural basis of USP30 inhibition

Key Words:

Mitophagy, Ubiquitin Specific Protease USP30, Benzosulfonamide, Activity-Based Protein Profiling, Enzyme Kinetics, Hydrogen Deuterium eXchange-Mass Spectrometry, Molecular Docking

## ABSTRACT

Dampening functional levels of the mitochondrial deubiquitylating enzyme USP30 has been suggested as an effective therapeutic strategy against neurodegenerative disorders such as Parkinson's Disease. USP30 inhibition may counteract the deleterious effects of impaired turnover of damaged mitochondria which is inherent to both familial and sporadic forms of the disease. Small-molecule inhibitors targeting USP30 are currently in development, but little is known about their precise nature of binding to the protein. We have integrated biochemical and structural approaches to gain novel mechanistic insights into USP30 inhibition by a small-molecule benzosulfonamide containing compound, **39**. Activity-based protein profiling (ABPP) mass spectrometry confirmed target engagement, the high selectivity, and potency of **39** for USP30 against 49 other deubiquitylating enzymes in a neuroblastoma cell line. *In vitro* characterization of **39** enzyme kinetics infers slow and tight binding behavior, which is comparable with features of covalent modification of USP30. Finally, we blended hydrogen-deuterium exchange mass spectrometry and computational docking to elucidate the molecular architecture and geometry of USP30 complex formation with **39**, identifying structural rearrangements at the cleft of the USP30 thumb and palm subdomains. These studies suggest that **39** binds to the thumb-palm cleft that guides the ubiquitin C-terminus into the active site, thereby preventing ubiquitin binding and isopeptide bond cleavage, and confirming its importance in the inhibitory process. Our data will pave the way for the design and development of next-generation inhibitors targeting USP30 and associated deubiquitinylases.

## INTRODUCTION

Ubiquitination is essential to protein quality control, homeostasis and lifespan.[1] Damaged proteins are flagged for removal from cells with the covalent addition of ubiquitin (Ub), a small, highly conserved 76-amino acid protein that is widely expressed across eukaryotic cell types.[2, 3] This molecular "kiss of death" proceeds through the coordinated action of E1, E2, and E3 ligase enzymes, with targeted

47 protein substrates conjugated by way of an isopeptide bond to either a single Ub molecule (mono-
48 ubiquitination), or several repeating units (poly-ubiquitination).[4] Besides the Ub-proteasome system
49 (UPS) subfamily, proteins selected for degradation can also be trafficked through the autophagy-
50 lysosome pathway. In damaged mitochondria, such autophagic clearance of impaired proteins occurs
51 through a highly selective and dedicated mechanism termed "mitophagy". Several key players work
52 tirelessly in the dysregulated mitochondrion to maintain overall cell integrity and survival, including
53 the mitochondrial outer membrane (MOM)-associated Ub serine/threonine kinase PINK1 and the
54 cytoplasmic E3 ligase Parkin.[5] PINK1 phosphorylates Ub species on damaged proteins accumulating
55 on the MOM, flagging them for elimination. This in turn recruits and activates endogenous Parkin (also
56 by phosphorylation), initiating a hyper-ubiquitination cascade that gives the green light for mitophagy
57 to proceed in a specialized autophagosome structure.[6] Deubiquitinating enzymes (DUBs) counteract
58 the actions of E3 ligases by removing Ub modifications, and several of these Ub-specific proteases
59 (USPs) have been shown to oppose Parkin activity.[7, 8] Of these, USP30 is the predominant active DUB
60 to be directly implicated in mitophagy to-date, primarily due to its localization on the MOM, whilst
61 also being linked to pexophagy and oxygen metabolism due to its widespread expression on
62 peroxisomes.[9] Interestingly, Parkin and USP30 both share an unusual preference for Lys6-linked Ub
63 chains, the mitophagic importance of which has yet to be conclusively deciphered.[10, 11]

64 Impaired mitophagy and oxidative stress have adverse roles in neurodegeneration, with both being
65 linked to familial and sporadic forms of Parkinson's Disease (PD)[12, 13]; PINK1/Parkin-mediated
66 mitophagy limits the build-up of toxic mitochondrial species in PD and loss-of-function mutations
67 occurring in the PINK1 and PRKN genes result in the progressive depletion of dopaminergic neurons
68 of the basal ganglia and a rare hereditary form of juvenile Parkinsonism.[14, 15] As USP30 antagonizes
69 mitophagy through ubiquitination, its inhibition has been proposed as a novel therapeutic strategy to
70 enhance mitochondrial turnover and clear damaged mitochondrial proteins, providing a much-needed
71 strategy to improve outcomes in PD and other neurodegenerative disorders. Several small-molecule
72 inhibitors targeting USP30 are in the pipeline, including phenylalanine derivatives, *N*-cyano

73 pyrrolidines and natural products.[16-18] Perhaps those with the greatest potential, however, are a family
74 of benzosulfonamides, most notably, compound **39**, which has been shown to boost mitophagy in
75 dopaminergic neurons of PD patients by down-regulating USP30.[19, 20] Little is currently known,
76 however, regarding the intricacies of its non-covalent attachment to USP30 itself, and the structural
77 basis of its inhibitory action. X-ray crystallography has recently provided structures of both human and
78 zebrafish USP30, but these are solely in the context of attachment to Lys6-linked di-Ub moieties.[10, 11]
79 Hydrogen/Deuterium eXchange Mass Spectrometry (HDX-MS) is a complementary biophysical tool
80 that can provide unique insights into protein structure, stability, dynamics and function.[21] In direct
81 contrast to the static snapshot provided by the crystal structure, HDX-MS monitors the conformational
82 dynamics of a system *in solution*, enabling the analysis of "proteins in motion". The technique has
83 shown particular utility for the rapid and reliable identification of small-molecule binding pockets on
84 proteins.[22] Whilst lacking the resolution of a crystal structure, the highly informative data obtained
85 from HDX-MS can be combined with orthogonal structural, computational, biochemical and/or
86 biophysical techniques to define structure activity relationships (SAR) and to direct drug discovery
87 campaigns.

88 As such, we have integrated several biophysical and structural approaches to help clarify the molecular
89 and structural interplay of **39** binding to USP30. The endogenous cellular selectivity of **39** for USP30
90 inhibition was confirmed using activity-based protein profiling mass spectrometry (ABPP-MS) against
91 a panel of 49 other endogenous DUBs in neuronal SH-SY5Y cells. Bio-layer interferometry showed that
92 **39** binds to USP30 in a slow and tight manner, which intriguingly, despite being a non-covalent binder,
93 is consistent with the profile of covalent inhibition. Finally, we combined HDX-MS and molecular
94 docking simulations to elucidate the conformational dynamics and spatial preferences of **39** binding,
95 identifying key residues in the inhibitory process itself. **39** induces conformational and structural
96 rearrangements at the cleft of the USP30 thumb and palm subdomains, in a region encompassing its
97 catalytic residues and the site of Ub binding. We postulate that these phenomena underlie the
98 mechanism of inhibition of **39**. Dampening USP30 pharmacologically may represent a tractable

99 treatment for PD and other mitophagy-related disorders. As no previous attempts to investigate the
100 molecular basis of compound **39** binding to USP30 have been reported, our data will be instrumental
101 in the development of rational next-generation inhibitors against USP30 and related DUBs.

102

103 **RESULTS AND DISCUSSION**

104 ***Compound 39 is highly potent and selective for neuronal USP30***

105 The efficacy and selectivity of compound **39** across a panel of cysteine active DUBs was initially
106 screened in SH-SY5Y neuroblastoma cell lysates by ABPP (**Figure 1a**). SH-SY5Y cell extracts were
107 treated with a range of inhibitor concentrations from 0.1 to 25 µM, followed by incubation with a HA-
108 tagged Ub-based probe with a propargylamine warhead (HA-Ub-PA). DUB probe complexes were
109 immunoprecipitated by way of their HA tag and quantified using label-free quantitation (LFQ) LC-
110 MS/MS. We implemented a data independent acquisition (DIA) MS regime to maximize the depth and
111 reproducibility of the DUB profiling assay.[23, 24] The concentration-dependent competition between
112 compound **39** and HA-Ub-PA for binding to USP30 confirmed target engagement and potency of the
113 inhibitor in a cellular matrix, with an $IC_{50}$ value in the nanomolar range (**Figure 1b**). Moreover, **39** was
114 found to be highly selective for USP30 as it had no significant activity against any of the other 49
115 endogenous DUBs detected in the experiment (**Figure 1b**). The main cysteine-reactive DUB enzyme
116 families were all represented, with proteins containing USP, ovarian tumor protease (OTU), Ub C-
117 terminal hydrolase (UCH), and Josephin domains quantified.[25, 26] The absence of **39** concentration-
118 dependent inhibition for all other identified cysteine active DUBs demonstrates the highly selective
119 nature of the inhibitor. This selectivity is in line with previously published USP30 inhibitor selectivity
120 data from both a recombinant DUB activity panel[20] and an ABPP-MS experiment on a smaller panel of
121 endogenous DUBs identified from mouse brain tissue.[27]

122 We have recently reported that **39** can be displaced by HA-Ub-PA over long incubations.[27] Accordingly,
123 a small amount of displacement during the 45 min HA-Ub-PA incubation was anticipated. It is
124 therefore expected that the $IC_{50}$ value of 0.16 µM that we obtained from our ABPP-MS assay is likely
125 higher than the absolute $IC_{50}$ inhibition concentration (**Figure 1c** and **d**).

126 ***Compound 39 binds USP30 in a slow and tight manner***

127 Once it was established that **39** down-regulates endogenous USP30 activity in a highly selective
128 fashion, we sought to rigorously profile its inhibitory properties using a recombinant version of the
129 protein. Synthetic full-length USP30 is very unstable and difficult to solubilize.[10] To circumvent this,
130 we used a previously described truncated version of USP30 in our enzyme (and HDX-MS) assays, which
131 readily went into solution and was determined to be stable over the time course of our experiments
132 (**Figure S1**). To assess enzyme deubiquitinating efficiency, the purified USP30 construct was incubated
133 with a fluorogenic Ub-rhodamine substrate in both the presence and absence of compound **39**. This
134 resulted in a calculated $IC_{50}$ value for **39** of ~2 nM *in vitro*, which was in-line (albeit 10-fold lower) with
135 previous estimations (**Figure 2a**).[19] Although both measurements remain in the nM range, the 2 nM
136 $IC_{50}$ from the Ub-rhodamine assay is lower than the 162 nM $IC_{50}$ from the ABPP. This could be
137 attributable to differences in the endogenous and recombinant activity of USP30, non-specific
138 inhibitor occlusion in the cellular context of the ABPP, or displacement of compound 39 in the ABPP
139 by HA-Ub-PA. Progress curves for Ub-rhodamine cleaved by USP30 were used to calculate the rate of
140 inhibition. The kinetic constants $k_5$, $k_6$ and $K_i$ gave values that were indicative of slow, tight binding
141 behavior (**Figures 2b**, **d**, **e** and **f**). The latter was visualized by a time-dependent shift of dose-response
142 inhibition curves (**Figure 2d**), as well as by plotting $IC_{50}$ values against time (**Figure 2e**). When
143 considering the binding Scheme A (**Experimental Section**), the small value for $k_6$ implies that it is
144 behaving in an irreversible manner. The progress curves show typical features of an enzyme reaction
145 in the presence of a slow binding inhibitor. Furthermore, two binding events are observed in the form

146 of a) an initial and b) a steady-state velocity – both of which need to be considered during curve fitting
147 and calculation of inhibitory rates (see **Equations 2** and **3** in **Supporting Information**) (**Figure 2b**).

148 Bio-layer interferometry experiments confirmed this slow and tight binding behavior (**Figure 2c**). The
149 compound had an association rate of 0.3 $mM^{-1}s^{-1}$ and a very slow dissociation from USP30 that was
150 comparable with features of covalent modification (**Figure 2f**). This phenomenon is intriguing, as **39** is
151 known to bind to USP30 (as shown by MS), by exclusively non-covalent means.

152 ***HDX-MS kinetics identifies key residues at the compound 39 binding interface of USP30***

153 Knowledge is currently lacking on the precise location and mechanistics of **39** binding to USP30. HDX-
154 MS experiments were consequently designed to pinpoint the key regions of **39** binding to USP30,
155 whilst providing novel structural insights into the solution conformation and dynamics of complex
156 formation. HDX relies on the natural isotopic exchange of the amide backbone hydrogens of a protein
157 with deuterium when placed in a deuterated solution.[21] This leads to protein mass increases that are
158 directly measurable by MS which can serve as direct probes of protein solvent accessibility and
159 structure. Shielding of the deuterated solvent following introduction of a binding partner is indicative
160 of a binding interface. We sought to identify such regions following **39** binding to USP30 by directly
161 comparing the differences in HDX-MS uptake patterns of USP30 before (apo-USP30; in the presence
162 of DMSO) and after (holo-USP30; in the presence of **39**) complex formation.

163 Following digestion of unlabeled USP30 with pepsin, a total of 723 peptides were generated for the
164 protein, 133 of which were shortlisted for downstream data analysis (**Figure S2**). Selected peptides
165 covered 96.2% of the USP30 sequence, with an average of 4.19 peptides covering each amino acid.
166 The kinetics of deuterium uptake was analysed for all regions of USP30, which included USP domains
167 1-6 and the catalytic triad at Cys77, His452 and Ser477 (**Figure S3a**). From three independent
168 replicates, the relative fractional exchange was calculated for all peptides at each of the four time
169 points 30, 60, 600, and 3600 sec, and plotted as a function of peptide position (**Figures 3a and S3b**).

170 Following incubation with compound **39** in conditions conducive to binary complex formation, our
171 comparative HDX-MS data indicate that the majority of USP30 is unaffected by inhibitor binding, with
172 no differences in deuterium uptake kinetics between apo- and holo-states (**Figure 3a**). This suggests
173 that **39** binding is confined to smaller subsections of the protein. Indeed, several short regions of
174 USP30 had significant shielding from the solvent in the presence of the inhibitor as compared to the
175 DMSO control, indicative of regions involved in compound binding (**Figures 3a** and **b**). The areas of
176 most significant perturbation included at two peptides spanning the USP30 catalytic Cys77 residue,
177 N72-L83 (labeled Regions I and II in **Figure 3** and highlighted in representative uptake plots in **Figure**
178 **3b**), in addition to peptides mapping to D145-M149 (Region IV), E158-F166 (Regions V and VI), I323-
179 L328 (Region VII), and finally, H449-Y456 (Region VIII), which encompasses the catalytic His452. These
180 were in direct contrast to Regions III and IX, which gave identical HDX-MS behaviors in both the apo-
181 and holo-form, reflecting the majority of the USP30 protein sequence (**Figure 3b**). The shielding
182 induced by inhibitor was greatest at the 1 h timepoint, where a difference of >25% was observed in
183 the relative fractional uptake between states. Results were confirmed by the presence of multiple
184 overlapping peptides displaying equivalent HDX-MS activity. Interestingly, no difference in
185 conformational dynamics was observed between states for the region covering the catalytic Ser477
186 (Region IX), suggesting that this site is not vital to the **39** inhibitory process, but rather, may have a
187 greater influence in determining USP30 Ub linkage preferences.[10, 11, 28] Nevertheless, targeting this site
188 to improve USP30 inhibition efficacies may prove fruitful in future design regimes.

189 No X-ray crystal structure of apo-USP30 or USP30 in complex with **39** currently exists. We therefore
190 mapped our solution HDX-MS data to PDB code 5OHK, which at a resolution of 2.34 Å, represents the
191 highest resolution 3D structure of the protein currently available in the Protein Data Bank (PDB).[10] It
192 is worth noting that this structure corresponds to USP30 in covalent complex with Lys6-linked di-Ub,
193 and as such, may give rise to subtle discrepancies when comparing across results. Nevertheless, due
194 to the lack of more suitable alternatives, we felt it a worthwhile pursuit to map our apo- and holo-
195 USP30 HDX-MS data to this 3D model. To facilitate a facile overview of the entire dataset, HDX-MS

196 results were collapsed into a single datapoint by calculating the mean perturbation between apo- and
197 holo-states across the four labeling time points. USP30 constitutes three subdomains designated
198 "thumb, palm and fingers", which is in line with related USP family members of elucidated structure.[7,
199 29] Strikingly, the shielded USP30 peptides in the presence of **39** all cluster to the same spatially
200 adjacent region of the protein, which lies at the interface of its palm and thumb subdomains (**Figure
201 3c**). Moreover, the regions with the greatest perturbation as highlighted above, I323-L328 (Region VII)
202 and H449-Y456 (Region VIII), cover areas of the protein which lie opposite each other on the 3D
203 structure. They may represent an entrance vector to the USP30 binding pocket, which is anticipated
204 to be closer to the site of greatest perturbation at E158-F166 (Regions V and VI) and the nearby
205 catalytic Cys77. The importance of these residues to the inhibitory process is further strengthened by
206 their correlation with the proposed region of USP30 binding to the Ub C-terminal tail in the crystal
207 structure.[10]

208 ***Binding of 39 alters USP30 conformation and induces rigidification in several regions***

209 Although likely to be in good agreement with the majority of 5OHK, the structural make-up of apo-
210 USP30 has yet to be experimentally confirmed. As yet, no high-resolution crystal structure exists,
211 which is of a direct consequence of the poor stability of the full-length protein itself.[10] As stated earlier,
212 a highly truncated USP30 construct was used in this study, which was devoid of its N-terminal
213 mitochondrial intermembrane domain and adjacent transmembrane domain. Furthermore, several
214 long, disordered regions were cleaved, and multiple hydrophobic residues mutated out, resulting in
215 substantially improved protein stability and solubility. As HDX-MS is not reliant on successful
216 crystallization trials, we saw this as an opportunity to describe the solution structural integrity of apo-
217 USP30, which would allow us to elucidate its mode of binding to **39**.

218 The conformational landscape of apo-USP30 generally follows the arrangement of its USP domains;
219 some of the most solvent exposed regions of the protein are found at the linker regions connecting
220 individual domains, most noticeably between USP domains 1 and 2, 4 and 5, and 5 and 6 (**Figures S3a**

221 **and S3b**). Conversely, USP domains 1 and 5 and the N-terminal end of USP domain 6 are largely
222 protected from the solvent and inaccessible (**Figure S3b**). This is in good agreement with HDX-MS data
223 recently acquired on the full length apo-USP30 protein, where the USP domains were shown to be in
224 a conformation that was generally hidden from the solvent and connected by several exposed
225 linkers.[10] However, due to the instability of the full-length species, HDX-MS was performed on a much
226 smaller scale compared to our own study, with only a sole 3 sec labeling time point measured.
227 Furthermore, an appreciation of USP30 dynamics could not be extracted from this single time point.
228 Looking at apo-USP30 dynamics across the several labeling time points described herein, an increase
229 in the rate of deuteration over the time course of the experiment was observed across the majority
230 of the protein (**Figure S3b**). This dynamic HDX-MS behavior is indicative of the presence of secondary
231 structural elements, thereby confirming the highly structured nature of the protein. The regions with
232 the greatest dynamic HDX-MS behavior were found within USP domains 2, 3, 4, and 6 (**Figure S3b**).
233 Conversely, no dynamic HDX-MS events were observed in several regions of apo-USP30 and the
234 maximum level of deuteration was reached immediately, indicating structural disorder. These
235 unstructured regions map to the N- and C-terminal extremities of the protein and within USP domains
236 1 (residues 71-78), 2 (residues 130-136), and 5 (residues 439-453). There is a high level of overlap
237 when mapping the structural data inferred from the HDX-MS to the crystal structure of 5OHK for both
238 apo- and holo-USP30 (**Figure S4**).

239 Several regions of USP30 undergo structural transitions in the presence of **39,** which are potentially
240 significant in terms of inhibitory mechanistics. First, multiple segments of USP30 become completely
241 blocked and inaccessible to the solvent following inhibitor binding. These include a region directly
242 adjacent to the catalytic Cys77 at F78-L83 and an area of USP domain 2 covering E158-F166, as
243 highlighted in purple in **Figure S4**. This suggests that **39** induces a conformation of USP30 that not only
244 blocks off the catalytic region and its surroundings from the solvent, but importantly, also prevents
245 access and binding of Ub itself. A second structural phenomenon is also evident, specifically the
246 conversion of intrinsically disordered loops in the absence of **39**, to rigid, structural elements in the

247 presence of the compound (**Figure S4**). These disorder-to-order transitions likely embody functional
248 significance[30] and in USP30, are found at the catalytic Cys77, represented by peptide V71-F78, a
249 section of USP domain 2 at R148-F154, and a long chain of residues spanning Q326-L349.

250 Tracking these structural rearrangements across individual labeling time points allows us to propose
251 a general timeline of inhibition (**Figure S5**). Taking Q326-L349 as an example, peptides mapping to this
252 region of USP30 undergo significant structural transitions at the earliest time points monitored (30
253 and 60 sec), which are completed in the later stages of our experimental time course. Conversely,
254 peptides proximal to the catalytic Cys77 become blocked and solvent inaccessible primarily in the
255 latter half of our experiment (600 and 3600 sec). The fact that the residue (and adjacent regions) most
256 crucial to USP30 catalysis, Cys77, is most significantly perturbed in the latter stages of our experiment
257 could go some way to explain the slow and tight binding behavior observed for **39** in our enzyme
258 kinetics analyses (**Figure 2**).

259 ***Molecular docking proposes key residues important for 39 binding to USP30***

260 To further refine our HDX-MS findings, we explored the binding mode of **39** to USP30 computationally.
261 We performed molecular docking simulations using the simple docking mode in AMDock software,
262 with the USP30 crystal structure 5OHK as the target receptor for the compound.[10, 19, 31] The *in silico*
263 binding pose of **39** with the highest-ranking docking score has estimated affinity and Ki values of -7.7
264 kcal/mol and 2.27 µM respectively, compared with a reported experimental $IC_{50}$ value of
265 approximately 20 nM.[19] Compound **39** is predicted to bind to the thumb-palm cleft that guides the Ub
266 C-terminus into the active site, residing approximately 7.9 Å away at its closest point from the thiol
267 side chain of catalytic Cys77 (**Figure 4a**). Compound **39** adopts a hydrophobic collapsed conformation
268 with an edge-to-face intramolecular pi-stacking interaction between the phenyl and fluorophenyl
269 moieties. **39** is predicted to form hydrogen bonding interactions between the carbonyl of the
270 fluorophenyl amide moiety and the side chain imidazole of His444, the amide of the phenylamide
271 moiety and the main chain carbonyl of Met448, and the sulfonamide moiety and the side chain

272 imidazole of His449 (**Figure 4b**). In addition, the fluorophenyl moiety is predicted to form an edge-to-
273 face π-stacking interaction with Tyr495. Compared with the structure of USP30 in complex with Ub-
274 PA (PDB code = 5OHK), the modelled position of **39** would sterically clash with the C-terminal tail of
275 the Ub substrate with the fluorophenyl moiety sitting in an equivalent position to the side chain of Ub
276 Leu73, thereby preventing Ub binding and isopeptide bond cleavage (**Figure 4c**).

277 Crystal structures of USP7 in complex with the small-molecule inhibitors, FT761 (PDB code= 5NGE)[29]
278 and GNE-6776 (PDB code= 5UQX)[32], reveal two distinct inhibitor binding modes that attenuate Ub
279 binding and inhibit the DUB activity. FT671 binds to the thumb-palm cleft and resides approximately
280 5 Å away from the catalytic cysteine whereas GNE-6776 interacts with acidic residues in the USP7
281 catalytic domain that mediate hydrogen-bonding interactions with the Ub Lys48 side chain and binds
282 12 Å from the catalytic cysteine. A comparison of the docked structure of **39** with the USP7 inhibitor
283 complexes suggests that **39** is most likely to bind to an equivalent site to FT671 (**Figure 4d**). In addition,
284 the docked pose of **39** correlates well with the HDX-MS data, with the predicted binding site of **39**
285 being flanked by residues residing in peptides E158-F166, I323-L328, and H449-Y456, which become
286 solvent protected in HDX-MS (**Figure 4a** and **b**). The HDX-MS analysis also implicates peptides N72-
287 L83 (which contains the catalytic Cys77) and D139-M149 in structural rearrangements upon
288 compound binding. These regions reside further from the predicted binding site of **39**. However,
289 compound binding may potentially cause conformational reorientation of the catalytic domain remote
290 from the binding site resulting in these regions becoming protected upon compound binding. Similar
291 conformational rearrangements are seen in human USP7, in which the inhibitors bind to the
292 catalytically incompetent apo-state with switching loop "in" as compared with the catalytically
293 competent Ub-bound state with switching loop "out", and it is possible that USP30 may exhibit similar
294 dynamic conformational flexibility**.**

295

296 **CONCLUSIONS**

297 Mitochondrial pathway disruption has been linked to a spectrum of pathophysiological conditions,
298 from neurodegeneration and acute, chronic kidney and cardiovascular diseases, through to
299 hepatocellular carcinoma and peroxisome biogenesis disorders.[6, 33-35] USP30 represents an actionable
300 drug target of these conditions through its participation in PINK1/Parkin-mediated mitophagy,
301 BAX/BAK-dependent apoptosis, oncogenesis, and pexophagy.[18, 36-38] USP30 regulates mitophagy by
302 antagonizing Parkin-mediated ubiquitination and its inhibition has been shown to have significant
303 therapeutic potential against PD and similar neurodegenerative disorders. Drug discovery efforts
304 targeting USP30 have yielded the highly potent and selective small-molecule benzosulfonamide
305 inhibitor, compound **39**.[17, 19, 39] Combining state-of-the-art proteomics, HDX-MS and molecular
306 docking, we have described the dynamic structural interplay between USP30 and **39**. The inhibitor
307 binds USP30 in a slow and tight manner, and displays kinetic properties consistent with covalent
308 attachment to USP30, despite its non-covalent design. Collectively, our integrative structural biology
309 lens successfully identified regions within USP30 that undergo dramatic structural and conformational
310 rearrangements in the presence of **39**, which prevent Ub binding and decrease DUB activity. X-ray
311 data for USP30 in complex with **39** will undoubtedly complement these observations and will,
312 combined with molecular dynamics studies, drive the development of next-generation inhibitors.

313

314 **EXPERIMENTAL SECTION**

315

316 **1. ABPP ASSAY**

317 ***HA-Ub-PA synthesis***

318 HA-Ub-PA synthesis was carried out as previously described.[27, 40] Briefly, a pTYB construct was used to
319 express Ub (Gly76del) in *E.coli*. The Ub was tagged with a HA tag on the N-terminus, and an intein-
320 chitin binding domain on the C terminus. *E.coli* lysis was performed using sonication in 50 mM Hepes,
321 150 mM NaCl, 0.5 mM Dithiothreitol (DTT). The protein was then bound to chitin bead slurry and
322 incubated with 100 mM MesNa overnight (37˚C with agitation) to form HA-Ub-MesNa. The HA-Ub-

323 MesNa was then incubated for 20 min with 250 mM propargylamine (PA; room temperature with
324 agitation), and desalted to remove excess propargylamine, resulting in the reactive activity-based
325 probe HA-Ub-PA.

326 ***Cell culture and lysis***

327 SH-SY5Y cells were cultured at 37˚C, 5% $CO_2$, in Eagle's Minimum Essential Medium and Ham's F12
328 Nutrient Mix (1:1), supplemented with 15% Fetal Bovine Serum, 1% non-essential amino acids and 2
329 mM Glutamax. Cells were collected by washing with phosphate-buffered saline (PBS), followed by
330 scraping in PBS and centrifugation at 200 x g. Cells were lysed in 50 mM Tris Base, 5 mM $MgCl_2.6\ H_2O$,
331 0.5 mM EDTA, 250 mM Sucrose, 1 mM DTT by vortexing with acid washed beads (1:1 v/v) 10 times (30
332 seconds vortexing, 1 min break on ice). Lysates were clarified at 600 x g for 10 min at 4˚C. Lysate
333 protein concentration was then determined by BCA.

334 ***Inhibitor selectivity with HA-Ub-PA immunoprecipitation***

335 HA-Ub-PA protein complexes were immunoprecipitated and analysed using LC-MS/MS as previously
336 described.[41] Inhibitor **39** or DMSO was incubated with 500 µg of SH-SH5Y protein lysate for 1 h at 37˚C.
337 HA-Ub-PA was then incubated with the **39**-treated lysates for 45 min at 37˚C at a protein ratio of 1:200
338 (w/w). The reaction was quenched with the addition of 0.4% SDS and 0.5% NP-40 (IGEPAL CA-630) and
339 diluted to 0.5 mg/mL with 50 mM Tris, 0.5% NP-40, 150 mM NaCl and 20 mM $MgCl_2.6\ H_2O$, pH 7.4.
340 HA-Ub-PA protein complexes were then immunoprecipitated using 150 µL of pre-washed Anti-HA
341 agarose slurry overnight at 4˚C with end-over-end rotation. The agarose slurry was then washed four
342 times and the HA-Ub-PA protein complexes were eluted using 110 µL of 2 x Laemmli buffer. To check
343 for efficient immunoprecipitation, 10 µL of the eluates were run on a western blot.

344 The remaining 100 µL of the eluates were reduced with 20 mM DTT for 10 min at 95˚C and alkylated
345 with 40 mM of iodoacetamide for 30 min at room temperature in the dark. Proteins were then
346 acidified to 1.2% phosphoric acid, diluted 6-fold with 90% methanol/100 mM TEAB, and

347 captured/washed on an S-trap column according to the standard protocol.[42] Proteins were digested
348 on the S-trap column with 2 µg of trypsin overnight at 37˚C. Eluted peptides were then dried and
349 resuspended in 2% acetonitrile (ACN), 0.1% formic acid.

350 ***LC-MS/MS***

351 Peptides were analysed using a Dionex Ultimate 3000 nano-ultra high pressure reversed-phase
352 chromatography system coupled on-line to an Orbitrap Fusion Lumos mass spectrometer (Thermo
353 Scientific). Samples were separated on an EASY-Spray PepMap RSLC C18 column (500 mm x 75 µm, 2
354 µm particle size; Thermo Scientific) over a 60 min gradient of 2-35% ACN in 5% DMSO, 0.1% formic
355 acid and at 250 nL/min. The column temperature was maintained at 50°C with the aid of a column
356 oven. The mass spectrometer was operated in positive polarity mode with a capillary temperature of
357 275°C. data-independent acquisition (DIA) mode was utilized for automated switching between MS
358 and MS/MS acquisition as described previously.[23] Fractions were loaded with adjusted sample
359 volumes to analyze ∼200 ng on column.

360 ***DIA-MS data processing and analysis***

361 Data was analysed using DIA-NN (version 1.8) with all settings as default. A *Homo sapiens* Uniprot
362 database (retrieved on 16/04/2021) was used for the analysis. Immunoprecipitations were carried out
363 in duplicate and any DUBs that were not present in both control samples and enriched > 5-fold when
364 compared to a no probe control, were discarded from the analysis. Identifications that were assigned
365 to multiple DUBs were not included in the analysis. MINDY3 was also removed from the dataset as it
366 was the lowest intensity, so may have been at the bottom of the instruments dynamic range and did
367 not produce stable values across the dataset. All MS raw files were deposited in PRIDE under the code
368 PXD036574.

369

370 **2. ENZYME KINETICS**

371 ***In Vitro USP30 Activity Assay***

372 Fluorescence intensity measurements were used to monitor the cleavage of a Ub-rhodamine (Ub-
373 Rho110) substrate. All activity assays were performed in black 384-well plates in 20 mM Tris-HCl, pH
374 8.0, 150 mM Potassium Glutamate, 0.1 mM TCEP and 0.03% Bovine Gamma Globulin with a final assay
375 volume of 20 µL. Compound $IC_{50}$ values for DUB inhibition were determined as previously described.[17]
376 Briefly, an 11-point dilution series of compounds were dispensed into black 384-well plates using an
377 Echo-550 Acoustic Liquid Handler (Beckman Coulter). USP30, 0.2 nM (residues 64-502Δ179-216 & 288-
378 305, Viva Biotech (Shanghai) Ltd.) was added and the plates preincubated for 30 min, 25 nM Ub-
379 Rho110 (Ubiquigent) was added to initiate the reaction and the fluorescence intensity was recorded
380 for 30 min on a Pherastar FSX ($\lambda_{Ex}$ = 485 nm, $\lambda_{Em}$ = 520 nm) (BMG Labtech). Initial rates were plotted
381 against compound concentration to determine $IC_{50}$. Data was processed using analysis tools from
382 Dotmatics (https://www.dotmatics.com/).

383 ***Kinetic assays - determination of kinetic parameters for slow-tight binding inhibitors***

384 Kinetic assays were performed in 384-well Sensoplate™ in 20 mM Tris-HCl, pH 8.0, 300 mM Potassium
385 Glutamate, 0.1 mM TCEP and 0.2% BGG with a final assay volume of 50 µL. An 11-point dilution series
386 of compound was dispensed into assay plates and 25 µL 2X Ub-Rho110 was added. The dispense
387 function of the FLIPR® Tetra (Molecular Devices) was used to add 25 µL 2X USP30 to give final assay
388 concentrations of 5 and 180 nM for USP30 and Ub-Rho110 respectively. The fluorescence signal of the
389 enzyme activity was monitored every 3 sec for 1800 sec ($\lambda_{Ex}$ = 470-495 nm, $\lambda_{Em}$ = 515-575 nm, camera
390 gain 70, exposure time 0.6 sec, excitation intensity 80%). Analysis was performed in GraphPad Prism
391 version 9.4.1 for Windows (Graphpad Software, La Jolla, California, USA; www.graphpad.com). The
392 time course data was normalized relative to enzyme in the absence of compound and used to generate
393 inhibition curves at each time point.

394 $$E + I \underset{k_4}{\overset{k_3[I]}{\rightleftharpoons}} E\text{-}I \underset{k_6}{\overset{k_5}{\rightleftharpoons}} E\text{-}I^*$$ **Scheme A**

395 As $IC_{50}$ values are time-dependent for compound **39** with no covalent labeling of USP30, shown by MS
396 (**Figure S1**), data were modelled to a slow-tight binding scheme (**Scheme A**). Fitting of progress curves
397 allows for calculation of relevant kinetic parameters (**Supporting Information**).

398 ***Bio-layer interferometry***

399 Bio-layer interferometry was performed on an Octet RED384® system (Sartorius) at 25°C in a buffer
400 containing 20 mM Tris-HCl (pH 8), 100 mM NaCl, 2 mM TCEP, 0.05% Tween and 1% DMSO. Biotinylated
401 USP30 (residues 64-502Δ179-216 & 288-305, Viva Biotech (Shanghai) Ltd.) was immobilized onto
402 Super Streptavidin (SSA) biosensors. After 60 sec baseline detection, the association of defined
403 concentrations of **39** (0-5 µM) was recorded over 300 sec followed by dissociation in buffer over 600
404 sec. Traces were normalised by double subtraction of baseline (no compound) and reference sensors
405 (no USP30, association and dissociation of compound) to correct for non-specific binding to the
406 sensors. Traces were analysed using the Octet Software (Version 11.2, Sartorius).

407

408 **3. HDX-MS**

409 ***HDX sample preparation***

410 USP30 was incubated in either the presence (holo-USP30) or absence (apo-USP30) of a two-fold molar
411 excess of **39**, ensuring that all complexes were fully formed and maintained over the course of the
412 labeling reaction. Before the HDX-MS experiments, labelling (L), equilibration (E) and quench (Q)
413 buffers were freshly prepared with $D_2O$ or $H_2O$, respectively (Buffers E and L: 50 mM HEPES, 400 mM
414 NaCl, 2.0 mM TCEP, 10% glycerol (v/v) at pH 7.2; Buffer Q: 50 mM potassium phosphate buffer, 2.0 M
415 guanidine hydrochloride at pH 2.30). The USP30 protein sample was supplied at 66 µM and was diluted
416 in Buffer E to a final concentration of 11 µM, which equates to 16 pmol injected onto the pepsin
417 column. Buffers E and L were equilibrated at 20°C, while the protein samples and Buffer Q were
418 equilibrated at 0°C.

419 ***HDX cyclic ion mobility mass spectrometry***

420 HDX-MS experiments were carried out on a fully automated HDX-2 system (supplied by Waters,
421 Milford USA) previously described by Brown and Wilson.[43] The exchange reaction was initiated by
422 diluting 3.5 µL protein sample with a concentration of 11 µM into 56.5 µL Buffer E for reference, or
423 Buffer L for $D_2O$ labeling, and incubated for several time points (0, 30, 60, 600 and 3600 sec). A
424 $D_2O/H_2O$ ratio in excess of 90% guaranteed that the kinetics favored unidirectional exchange.
425 Subsequently, the exchange reaction was stopped by mixing 50 µL of sample with 50 µL pre-cooled
426 Buffer Q. Next, 50 µL of quenched sample was subjected to a temperature-controlled chromatography
427 system (HDX M-Class UPLC, Waters). The protein was digested online by a pepsin column (Enzymate
428 BEH pepsin column; 2.1 x 30 mm; Waters). Eluting peptides were trapped and washed on a C18 pre–
429 column (C18 1.7 µM VanGuard 2.1 x 5 mm pre-column; Waters) at 100 µL/min for 3 min and separated
430 on a reversed phase column (C18 1.7 µM Acquity UPLC 1 x 100 mm reverse phased column; Waters)
431 with a linear gradient ranging from 5% ACN to 40% ACN plus 0.2% FA at 40 µL/min in 8 min, followed
432 by a rapid rise to 99% ACN holding for 0.3 min. ACN concentration was rapidly reduced to 5% and held
433 there for 0.2 min, followed by a linear gradient back to 99% over 0.7 min, and holding that
434 concentration for 0.1 min. Next, C18 columns were equilibrated with 95% $H_2O$ plus 0.2% FA for 4 min.
435 The reversed-phase chromatographic system was kept at approximately 0°C to reduce back-exchange.
436 Peptides eluting from reversed phase column were measured with a SELECT SERIES Cyclic IMS mass
437 spectrometer (Waters, Wilmslow UK) in $HDMS^E$ mode (*m/z* 50-2000). This mode utilises ion mobility
438 (IM) separation for orthogonal separation of the peptides (LC, IM, *m/z*). The mass spectrometer was
439 fitted with an electrospray source equipped with additional independent LockSpray probe (Leu-
440 enkephalin LockMass solution was used, *m/z* 556.2771).

441 ***HDX-MS data processing and analysis***

442 All MS-analyses were performed in triplicate for each time point and condition. Protein Lynx Global
443 Server (PLGS) 3.0 (Waters Corporation) was used for peptide identifications. A peptic peptide

444 sequence coverage map was generated in DynamX 3.0 HDX software (Waters Corporation). Peptide-
445 level deuterium uptake data was also visualized in DynamX and reported as relative deuterium
446 exchange levels expressed in either mass unit or fractional exchange. The latter was calculated by
447 dividing the experimentally measured uptake by the theoretically maximum number of exchangeable
448 backbone amide hydrogens that could be replaced within each peptide. This number corresponds to
449 the number of amino acid residues present in the peptide minus the number of proline residues and
450 minus one for the N-terminus that back exchanges too rapidly to be measured by MS.[30] A single charge
451 state was considered per peptide. Data were also verified and visualized in MEMHDX.[44]

452

453 **4. MOLECULAR DOCKING**

454 The crystal structure of human USP30 catalytic domain (residues K64-V502) in covalent complex with
455 Ub-PA at 2.34 Å resolution represents the highest resolution human USP30 structure available in the
456 Protein Data Bank (PDB code= 5OHK)[10], and was used as the target receptor for docking the selective
457 USP30 benzosulfonamide inhibitor, compound **39**[19], using AutoDock Vina implemented in the program
458 AMDock 1.5.2.[31] Coordinates for **39** were generated using ChemDraw Prime 16.0.1.4, and PRODRG
459 implemented in the CCP4 software suite.[45] The compound was docked using the simple docking mode
460 and automatic defined search space in AMDock 1.5.2.

461

462 **FIGURE LEGENDS**

463 **Figure 1. Compound 39 is highly potent and selective for USP30 inhibition in a cellular context.** (a)
464 Chemical structure of **39**.[27] (b) Compound **39** is a highly selective USP30 inhibitor. (c) **39** acts in a
465 concentration dependent manner (down to 0.1 µM levels), which is in concordance with previously
466 published data for both mouse brain and with a recombinant DUBprofiler™ (Ubiquigent) panel. (d)
467 SHSY5Y cells were incubated with **39** for 1 h at 37˚C. The HA-Ub-PA was then incubated with **39**-
468 treated lysates for 45 min at 37˚C at a protein ratio of 1:200 (w/w) and immunoblotted as shown.
469 Engagement of USP30 with the probe was confirmed using anti-USP30 and anti-HA antibodies.

470 **Figure 2. Kinetic profiling of the non-covalent USP30 inhibitor 39.** Upper panel: (a) Dose dependent
471 inhibition of USP30 by **39**. (b) Reaction progress curves recorded on the FLIPR® Tetra. Traditional
472 method for determining kinetic constants associated with a two-step slow, tight binding inhibitor. $k_{obs}$,
473 determined by fitting the progress curves to Eq. 2 (**Supporting Information**), is plotted vs [Compound]
474 and fitted to Eq. 3. (**Supporting Information**) to determine $K_i$, $k_5$ and $k_6$. (c) Bio-layer interferometry
475 showing binding of **39** to immobilized USP30 with no detectable dissociation. Lower panel: (d)
476 Krippendorf method[46] (**Supporting Information**) was used as an alternative way of determining kinetic
477 constants. Time-dependent $IC_{50}$ curves. Each curve represents inhibition data at an individual
478 incubation time from 3-1800 sec. (e) $IC_{50}$ values vs. incubation time fitted to Eq. 1. (**Supporting**
479 **Information**) to obtain $K_i$ and $k_{inact}$. As **39** is non-covalent compound but has a $k_6$ which is essentially
480 0, $k_{inact}$ in this case represents $k_5$. (f) Data table of inhibition properties.

481 **Figure 3. HDX-MS characterises the conformational dynamics of compound 39 binding to USP30.** (a)
482 Residue-level heat map indicating that compound **39** induces solvent protection in several regions of
483 USP30. The plot displays the difference in relative fractional uptake between the holo- and apo-form
484 of the protein over 1 h. Regions of which have the greatest perturbation following **39** binding are
485 labeled Regions I-IX (b) Comparative uptake plots of Regions I-IX for apo- and holo-USP30 states (c)
486 Integrated HDX-MS and X-Ray crystal structure of USP30 in complex with di-Ub. Regions of
487 perturbation between apo- and holo-USP30 states HDX-MS data are colored according to magnitude
488 of change. The data indicates that the **39** binding interface is located between the USP30 thumb and
489 palm domains of the protein. Numbering is in accordance with the crystal structure of 5OHK. Dotted
490 lines indicate the site of cleavage and removal of unstable, disordered sequences from the full-length
491 USP30 protein.

492 **Figure 4. Modelled structure of human USP30 in complex with 39**. (a) Structure of human USP30
493 catalytic domain highlighting the modelled position of **39** shown as a stick representation and colored
494 green. The thumb, palm and fingers subdomains of the catalytic domain and catalytic triad (Cys77,
495 Ser477 and His42; underlined) are highlighted. Regions identified in the HDX-MS analysis of USP30 in
496 the presence of **39** are colored red. (b) Close-up view of the putative **39** binding site highlighting key
497 residues and hydrogen-bonding interactions represented as dotted lines. (c) Superposition of Ub-PA
498 (orange; PDB code= 5OHK) on the docked structure. **39** sterically clashes with the C-terminal tail of
499 the Ub substrate thereby preventing Ub binding and isopeptide bond cleavage. (d) Superposition of
500 the USP7 inhibitors, FT671 (yellow carbon atoms) and GNE-6776 (magenta carbon atoms) in complex
501 with USP7, onto the docked structure. **39** putatively binds to an equivalent site in the thumb-palm
502 cleft compared with FT671. Figure prepared using PyMOL (The PyMOL Molecular Graphics System,
503 Version 2.4.1, Schrödinger, LLC.).

504

505 **ANCILLARY INFORMATION**

506 ***Supporting Information***

507 *This can be accessed here xxx*

508 ***PDB ID Codes***

509 *5OHK* represents the crystal structure of human USP30 catalytic domain (residues K64-V502) in
510 covalent complex with Ub propargylamide (Ub-PA) at 2.34 Å resolution. This is the highest resolution
511 structure of human USP30 currently available in the PDB.

512 ***Homology Models***

513 *Not applicable*

514 ***Corresponding Author Information***

515 *Dr Darragh P O'Brien can be contacted at darragh.obrien@ndm.ox.ac.uk*

516 *Professor Benedikt M Kessler can be contacted at benedict.kessler@ndm.ox.ac.uk*

517 ***Present/Current Author Addresses***

518 *Target Discovery Institute, Centre for Medicines Discovery, Nuffield Department of Medicine,*
519 *University of Oxford, UK* - Darragh P O'Brien, Hannah BL Jones, Benedikt M Kessler

520 *ARUK-Oxford Drug Discovery Institute, Centre for Medicines Discovery, Nuffield Department of*
521 *Medicine, University of Oxford, UK* - Franziska Guenther, Katherine S England, Emma J Murphy, Paul
522 Brennan, John B Davis

523 *Chinese Academy of Medical Sciences – Oxford Institute, Nuffield Department of Medicine, University*
524 *of Oxford, UK* - Adán Pinto-Fernández, Benedikt M Kessler

525 *Waters Corporation, Wilmslow, Cheshire, UK* - Malcolm Anderson

526 *Cancer Research Horizons, Francis Crick Institute, London, UK* - Andrew P Turnbull

527 ***Author Contributions***

528 JD and BMK designed the study. DPOB, HBLJ, FG, EM, MA, APT, and BMK wrote the first manuscript
529 draft. DPOB, HBLJ, FG, EM, APF, and MA designed and performed the experiments. APT designed and

530 performed the molecular docking. All authors discussed the results and commented on the
531 manuscript.

532 ***Acknowledgments***

533 We wish to express thanks to Drs Roman Fischer and Iolanda Vendrell from the Oxford Discovery
534 Proteomics Facility for their help with ABPP-MS data acquisition. We would like to thank Daryl S Walter
535 from Evotec and Jeff Schkeryantz from Bristol Myers Squibb for their highly useful project discussions.
536 Our gratitude goes to Alzheimer's Research UK for their support and funding for the ARUK-Oxford
537 Drug Discovery Institute (grant no. ARUK-2021DDI-OX). We would also like to thank our other funders,
538 including the Chinese Academy of Medical Sciences (CAMS) Innovation Fund for Medical Science
539 (CIFMS), China (grant number: 2018-I2M-2-002) (BMK, APF), Bayer (BMK), the late Mr & Mrs James
540 Hardwick for funding the ODDI Medicinal Chemistry Team and also the G & K Boyes Charitable Trust.

541 ***Abbreviations Used***

542 Ub, Ubiquitin; UPS, Ubiquitin Proteasome System; PD, Parkinson's Disease; MOM, Mitochondrial
543 Outer Membrane; SAR, Structure Activity Relationship; USP30, Ubiquitin Specific Protease 30; DUB,
544 Deubiquitinase; ABPP-MS, Activity-Based Protein Profiling Mass Spectrometry; LFQ, Label-Free
545 Quantitation; DIA, Data Independent Acquisition; HDX-MS, Hydrogen Deuterium eXchange Mass
546 Spectrometry; PDB, Protein Data Bank.

547

548 **REFERENCES**

549 1. Popovic, D.; Vucic, D.; Dikic, I., Ubiquitination in disease pathogenesis and treatment. *Nat*
550 *Med* **2014,** *20* (11), 1242-53.
551 2. Ciechanover, A., The ubiquitin proteolytic system and pathogenesis of human diseases: a
552 novel platform for mechanism-based drug targeting. *Biochem Soc Trans* **2003,** *31* (2), 474-81.
553 3. Pickart, C. M.; Eddins, M. J., Ubiquitin: structures, functions, mechanisms. *Biochim Biophys*
554 *Acta* **2004,** *1695* (1-3), 55-72.
555 4. Mulder, M. P.; Witting, K.; Berlin, I.; Pruneda, J. N.; Wu, K. P.; Chang, J. G.; Merkx, R.; Bialas,
556 J.; Groettrup, M.; Vertegaal, A. C.; Schulman, B. A.; Komander, D.; Neefjes, J.; El Oualid, F.; Ovaa,
557 H., A cascading activity-based probe sequentially targets E1-E2-E3 ubiquitin enzymes. *Nat Chem Biol*
558 **2016,** *12* (7), 523-30.
559 5. Pollock, L.; Jardine, J.; Urbe, S.; Clague, M. J., The PINK1 repertoire: Not just a one trick pony.
560 *Bioessays* **2021,** *43* (11), e2100168.
561 6. Bingol, B.; Sheng, M., Mechanisms of mitophagy: PINK1, Parkin, USP30 and beyond. *Free Radic*
562 *Biol Med* **2016,** *100*, 210-222.
563 7. Komander, D.; Clague, M. J.; Urbe, S., Breaking the chains: structure and function of the
564 deubiquitinases. *Nat Rev Mol Cell Biol* **2009,** *10* (8), 550-63.
565 8. Nguyen, T. N.; Padman, B. S.; Lazarou, M., Deciphering the Molecular Signals of PINK1/Parkin
566 Mitophagy. *Trends Cell Biol* **2016,** *26* (10), 733-744.

9. Marcassa, E.; Kallinos, A.; Jardine, J.; Rusilowicz-Jones, E. V.; Clague, M. J.; Urbe, S., New aspects of USP30 biology in the regulation of pexophagy. *Autophagy* **2019,** *15* (9), 1634-1637.
10. Gersch, M.; Gladkova, C.; Schubert, A. F.; Michel, M. A.; Maslen, S.; Komander, D., Mechanism and regulation of the Lys6-selective deubiquitinase USP30. *Nat Struct Mol Biol* **2017,** *24* (11), 920-930.
11. Sato, Y.; Okatsu, K.; Saeki, Y.; Yamano, K.; Matsuda, N.; Kaiho, A.; Yamagata, A.; Goto-Ito, S.; Ishikawa, M.; Hashimoto, Y.; Tanaka, K.; Fukai, S., Structural basis for specific cleavage of Lys6-linked polyubiquitin chains by USP30. *Nat Struct Mol Biol* **2017,** *24* (11), 911-919.
12. Pickrell, A. M.; Youle, R. J., The roles of PINK1, parkin, and mitochondrial fidelity in Parkinson's disease. *Neuron* **2015,** *85* (2), 257-73.
13. Agarwal, S.; Muqit, M. M. K., PTEN-induced kinase 1 (PINK1) and Parkin: Unlocking a mitochondrial quality control pathway linked to Parkinson's disease. *Curr Opin Neurobiol* **2022,** *72*, 111-119.
14. Kitada, T.; Asakawa, S.; Hattori, N.; Matsumine, H.; Yamamura, Y.; Minoshima, S.; Yokochi, M.; Mizuno, Y.; Shimizu, N., Mutations in the parkin gene cause autosomal recessive juvenile parkinsonism. *Nature* **1998,** *392* (6676), 605-8.
15. Valente, E. M.; Abou-Sleiman, P. M.; Caputo, V.; Muqit, M. M.; Harvey, K.; Gispert, S.; Ali, Z.; Del Turco, D.; Bentivoglio, A. R.; Healy, D. G.; Albanese, A.; Nussbaum, R.; Gonzalez-Maldonado, R.; Deller, T.; Salvi, S.; Cortelli, P.; Gilks, W. P.; Latchman, D. S.; Harvey, R. J.; Dallapiccola, B.; Auburger, G.; Wood, N. W., Hereditary early-onset Parkinson's disease caused by mutations in PINK1. *Science* **2004,** *304* (5674), 1158-60.
16. Yue, W.; Chen, Z.; Liu, H.; Yan, C.; Chen, M.; Feng, D.; Yan, C.; Wu, H.; Du, L.; Wang, Y.; Liu, J.; Huang, X.; Xia, L.; Liu, L.; Wang, X.; Jin, H.; Wang, J.; Song, Z.; Hao, X.; Chen, Q., A small natural molecule promotes mitochondrial fusion through inhibition of the deubiquitinase USP30. *Cell Res* **2014,** *24* (4), 482-96.
17. Rusilowicz-Jones, E. V.; Jardine, J.; Kallinos, A.; Pinto-Fernandez, A.; Guenther, F.; Giurrandino, M.; Barone, F. G.; McCarron, K.; Burke, C. J.; Murad, A.; Martinez, A.; Marcassa, E.; Gersch, M.; Buckmelter, A. J.; Kayser-Bricker, K. J.; Lamoliatte, F.; Gajbhiye, A.; Davis, S.; Scott, H. C.; Murphy, E.; England, K.; Mortiboys, H.; Komander, D.; Trost, M.; Kessler, B. M.; Ioannidis, S.; Ahlijanian, M. K.; Urbe, S.; Clague, M. J., USP30 sets a trigger threshold for PINK1-PARKIN amplification of mitochondrial ubiquitylation. *Life Sci Alliance* **2020,** *3* (8).
18. Wang, F.; Gao, Y.; Zhou, L.; Chen, J.; Xie, Z.; Ye, Z.; Wang, Y., USP30: Structure, Emerging Physiological Role, and Target Inhibition. *Front Pharmacol* **2022,** *13*, 851654.
19. Kluge, A. F.; Lagu, B. R.; Maiti, P.; Jaleel, M.; Webb, M.; Malhotra, J.; Mallat, A.; Srinivas, P. A.; Thompson, J. E., Novel highly selective inhibitors of ubiquitin specific protease 30 (USP30) accelerate mitophagy. *Bioorg Med Chem Lett* **2018,** *28* (15), 2655-2659.
20. Rusilowicz-Jones, E. V.; Barone, F. G.; Lopes, F. M.; Stephen, E.; Mortiboys, H.; Urbe, S.; Clague, M. J., Benchmarking a highly selective USP30 inhibitor for enhancement of mitophagy and pexophagy. *Life Sci Alliance* **2022,** *5* (2).
21. Engen, J. R.; Wales, T. E., Analytical Aspects of Hydrogen Exchange Mass Spectrometry. *Annu Rev Anal Chem (Palo Alto Calif)* **2015,** *8*, 127-48.
22. Marciano, D. P.; Dharmarajan, V.; Griffin, P. R., HDX-MS guided drug discovery: small molecules and biopharmaceuticals. *Curr Opin Struct Biol* **2014,** *28*, 105-11.
23. Demichev, V.; Messner, C. B.; Vernardis, S. I.; Lilley, K. S.; Ralser, M., DIA-NN: neural networks and interference correction enable deep proteome coverage in high throughput. *Nat Methods* **2020,** *17* (1), 41-44.
24. Jones, H. B. L.; Heilig, R.; Davis, S.; Fischer, R.; Kessler, B. M.; Pinto-Fernandez, A., ABPP-HT*-Deep Meets Fast for Activity-Based Profiling of Deubiquitylating Enzymes Using Advanced DIA Mass Spectrometry Methods. *Int J Mol Sci* **2022,** *23* (6).
25. Komander, D., Mechanism, specificity and structure of the deubiquitinases. *Subcell Biochem* **2010,** *54*, 69-87.

618 26. Clague, M. J.; Urbe, S.; Komander, D., Breaking the chains: deubiquitylating enzyme specificity
619 begets function. *Nat Rev Mol Cell Biol* **2019,** *20* (6), 338-352.
620 27. Jones, H. B. L.; Heilig, R.; Fischer, R.; Kessler, B. M.; Pinto-Fernandez, A., ABPP-HT - High-
621 Throughput Activity-Based Profiling of Deubiquitylating Enzyme Inhibitors in a Cellular Context. *Front*
622 *Chem* **2021,** *9*, 640105.
623 28. Cunningham, C. N.; Baughman, J. M.; Phu, L.; Tea, J. S.; Yu, C.; Coons, M.; Kirkpatrick, D. S.;
624 Bingol, B.; Corn, J. E., USP30 and parkin homeostatically regulate atypical ubiquitin chains on
625 mitochondria. *Nat Cell Biol* **2015,** *17* (2), 160-9.
626 29. Turnbull, A. P.; Ioannidis, S.; Krajewski, W. W.; Pinto-Fernandez, A.; Heride, C.; Martin, A. C.
627 L.; Tonkin, L. M.; Townsend, E. C.; Buker, S. M.; Lancia, D. R.; Caravella, J. A.; Toms, A. V.; Charlton,
628 T. M.; Lahdenranta, J.; Wilker, E.; Follows, B. C.; Evans, N. J.; Stead, L.; Alli, C.; Zarayskiy, V. V.;
629 Talbot, A. C.; Buckmelter, A. J.; Wang, M.; McKinnon, C. L.; Saab, F.; McGouran, J. F.; Century, H.;
630 Gersch, M.; Pittman, M. S.; Marshall, C. G.; Raynham, T. M.; Simcox, M.; Stewart, L. M. D.;
631 McLoughlin, S. B.; Escobedo, J. A.; Bair, K. W.; Dinsmore, C. J.; Hammonds, T. R.; Kim, S.; Urbe, S.;
632 Clague, M. J.; Kessler, B. M.; Komander, D., Molecular basis of USP7 inhibition by selective small-
633 molecule inhibitors. *Nature* **2017,** *550* (7677), 481-486.
634 30. O'Brien, D. P.; Durand, D.; Voegele, A.; Hourdel, V.; Davi, M.; Chamot-Rooke, J.; Vachette,
635 P.; Brier, S.; Ladant, D.; Chenal, A., Calmodulin fishing with a structurally disordered bait triggers CyaA
636 catalysis. *PLoS Biol* **2017,** *15* (12), e2004486.
637 31. Valdes-Tresanco, M. S.; Valdes-Tresanco, M. E.; Valiente, P. A.; Moreno, E., AMDock: a
638 versatile graphical tool for assisting molecular docking with Autodock Vina and Autodock4. *Biol Direct*
639 **2020,** *15* (1), 12.
640 32. Kategaya, L.; Di Lello, P.; Rouge, L.; Pastor, R.; Clark, K. R.; Drummond, J.; Kleinheinz, T.;
641 Lin, E.; Upton, J. P.; Prakash, S.; Heideker, J.; McCleland, M.; Ritorto, M. S.; Alessi, D. R.; Trost, M.;
642 Bainbridge, T. W.; Kwok, M. C. M.; Ma, T. P.; Stiffler, Z.; Brasher, B.; Tang, Y.; Jaishankar, P.; Hearn,
643 B. R.; Renslo, A. R.; Arkin, M. R.; Cohen, F.; Yu, K.; Peale, F.; Gnad, F.; Chang, M. T.; Klijn, C.;
644 Blackwood, E.; Martin, S. E.; Forrest, W. F.; Ernst, J. A.; Ndubaku, C.; Wang, X.; Beresini, M. H.; Tsui,
645 V.; Schwerdtfeger, C.; Blake, R. A.; Murray, J.; Maurer, T.; Wertz, I. E., USP7 small-molecule inhibitors
646 interfere with ubiquitin binding. *Nature* **2017,** *550* (7677), 534-538.
647 33. Honsho, M.; Okumoto, K.; Tamura, S.; Fujiki, Y., Peroxisome Biogenesis Disorders. *Adv Exp*
648 *Med Biol* **2020,** *1299*, 45-54.
649 34. Schmidt, M. F.; Gan, Z. Y.; Komander, D.; Dewson, G., Ubiquitin signalling in
650 neurodegeneration: mechanisms and therapeutic opportunities. *Cell Death Differ* **2021,** *28* (2), 570-
651 590.
652 35. Pan, W.; Wang, Y.; Bai, X.; Yin, Y.; Dai, L.; Zhou, H.; Wu, Q.; Wang, Y., Deubiquitinating
653 enzyme USP30 negatively regulates mitophagy and accelerates myocardial cell senescence through
654 antagonism of Parkin. *Cell Death Discov* **2021,** *7* (1), 187.
655 36. Bingol, B.; Tea, J. S.; Phu, L.; Reichelt, M.; Bakalarski, C. E.; Song, Q.; Foreman, O.;
656 Kirkpatrick, D. S.; Sheng, M., The mitochondrial deubiquitinase USP30 opposes parkin-mediated
657 mitophagy. *Nature* **2014,** *510* (7505), 370-5.
658 37. Liang, J. R.; Martinez, A.; Lane, J. D.; Mayor, U.; Clague, M. J.; Urbe, S., USP30 deubiquitylates
659 mitochondrial Parkin substrates and restricts apoptotic cell death. *EMBO Rep* **2015,** *16* (5), 618-27.
660 38. Riccio, V.; Demers, N.; Hua, R.; Vissa, M.; Cheng, D. T.; Strilchuk, A. W.; Wang, Y.;
661 McQuibban, G. A.; Kim, P. K., Deubiquitinating enzyme USP30 maintains basal peroxisome abundance
662 by regulating pexophagy. *J Cell Biol* **2019,** *218* (3), 798-807.
663 39. Harrigan, J. A.; Jacq, X.; Martin, N. M.; Jackson, S. P., Deubiquitylating enzymes and drug
664 discovery: emerging opportunities. *Nat Rev Drug Discov* **2018,** *17* (1), 57-78.
665 40. Borodovsky, A.; Ovaa, H.; Kolli, N.; Gan-Erdene, T.; Wilkinson, K. D.; Ploegh, H. L.; Kessler,
666 B. M., Chemistry-based functional proteomics reveals novel members of the deubiquitinating enzyme
667 family. *Chem Biol* **2002,** *9* (10), 1149-59.

668 41. Pinto-Fernandez, A.; Davis, S.; Schofield, A. B.; Scott, H. C.; Zhang, P.; Salah, E.; Mathea, S.;
669 Charles, P. D.; Damianou, A.; Bond, G.; Fischer, R.; Kessler, B. M., Comprehensive Landscape of Active
670 Deubiquitinating Enzymes Profiled by Advanced Chemoproteomics. *Front Chem* **2019,** *7*, 592.
671 42. HaileMariam, M.; Eguez, R. V.; Singh, H.; Bekele, S.; Ameni, G.; Pieper, R.; Yu, Y., S-Trap, an
672 Ultrafast Sample-Preparation Approach for Shotgun Proteomics. *J Proteome Res* **2018,** *17* (9), 2917-
673 2924.
674 43. Brown, K. A.; Wilson, D. J., Bottom-up hydrogen deuterium exchange mass spectrometry: data
675 analysis and interpretation. *Analyst* **2017,** *142* (16), 2874-2886.
676 44. Hourdel, V.; Volant, S.; O'Brien, D. P.; Chenal, A.; Chamot-Rooke, J.; Dillies, M. A.; Brier, S.,
677 MEMHDX: an interactive tool to expedite the statistical validation and visualization of large HDX-MS
678 datasets. *Bioinformatics* **2016,** *32* (22), 3413-3419.
679 45. Winn, M. D.; Ballard, C. C.; Cowtan, K. D.; Dodson, E. J.; Emsley, P.; Evans, P. R.; Keegan, R.
680 M.; Krissinel, E. B.; Leslie, A. G.; McCoy, A.; McNicholas, S. J.; Murshudov, G. N.; Pannu, N. S.;
681 Potterton, E. A.; Powell, H. R.; Read, R. J.; Vagin, A.; Wilson, K. S., Overview of the CCP4 suite and
682 current developments. *Acta Crystallogr D Biol Crystallogr* **2011,** *67* (Pt 4), 235-42.
683 46. Krippendorff, B. F.; Neuhaus, R.; Lienau, P.; Reichel, A.; Huisinga, W., Mechanism-based
684 inhibition: deriving K(I) and k(inact) directly from time-dependent IC(50) values. *J Biomol Screen* **2009,**
685 *14* (8), 913-23.

686

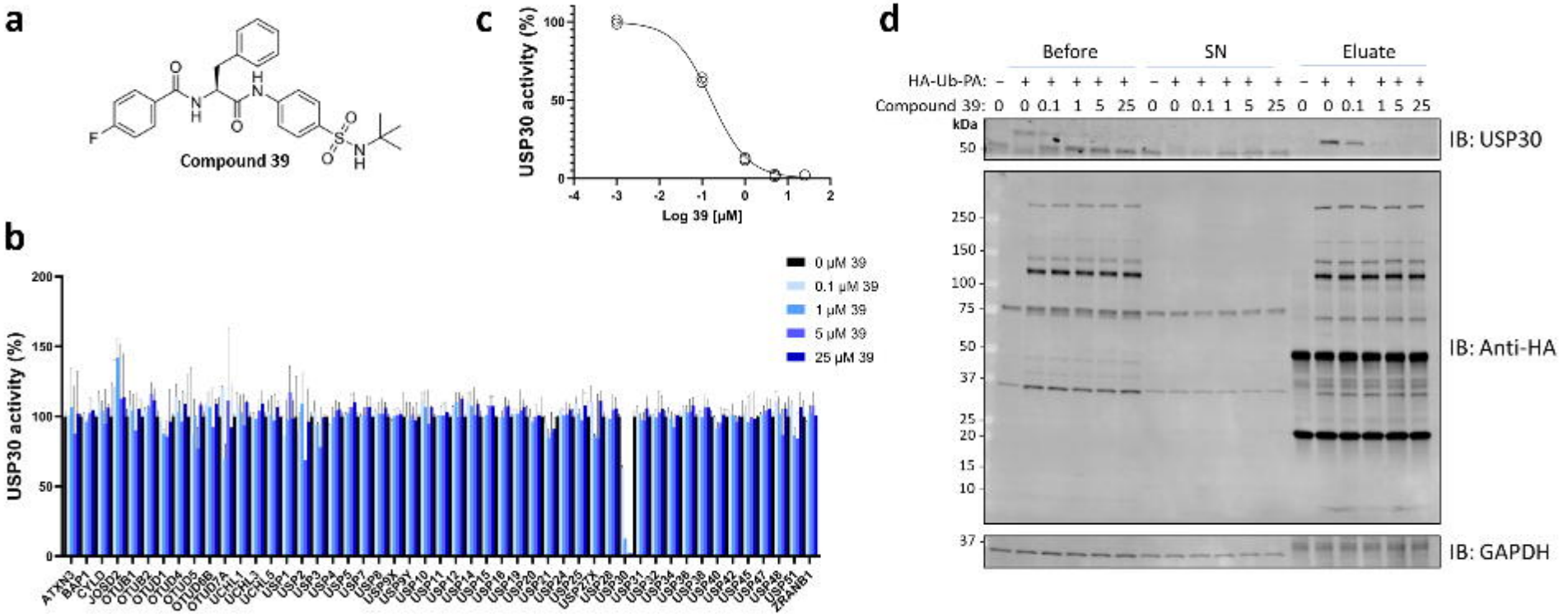
a
Compound 39
b
USP30 activity (%)
0 μM 39
0.1 μM 39
1 μM 39
5 μM 39
25 μM 39
ATXN3
BAP1
CYLD
JOSD2
OTUB1
OTUB2
OTUD1
OTUD4
OTUD5
OTUD6B
OTUD7A
UCHL1
UCHL3
UCHL5
USP1
USP2
USP3
USP4
USP5
USP7
USP8
USP9X
USP9Y
USP10
USP11
USP12
USP14
USP16
USP18
USP19
USP20
USP21
USP24
USP25
USP27X
USP28
USP30
USP31
USP32
USP34
USP36
USP38
USP40
USP42
USP45
USP47
USP48
USP51
ZRANB1
c
USP30 activity (%)
Log 39 [μM]
d
Before
SN
Eluate
HA-Ub-PA:
Compound 39:
kDa
IB: USP30
IB: Anti-HA
IB: GAPDH

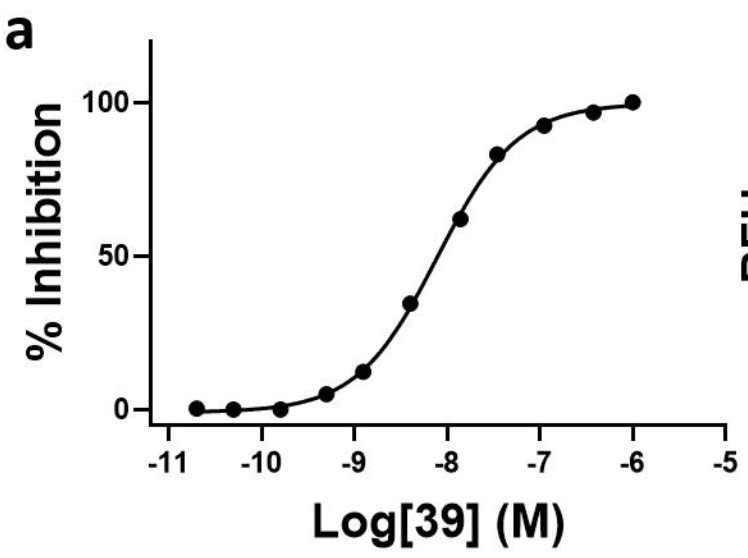


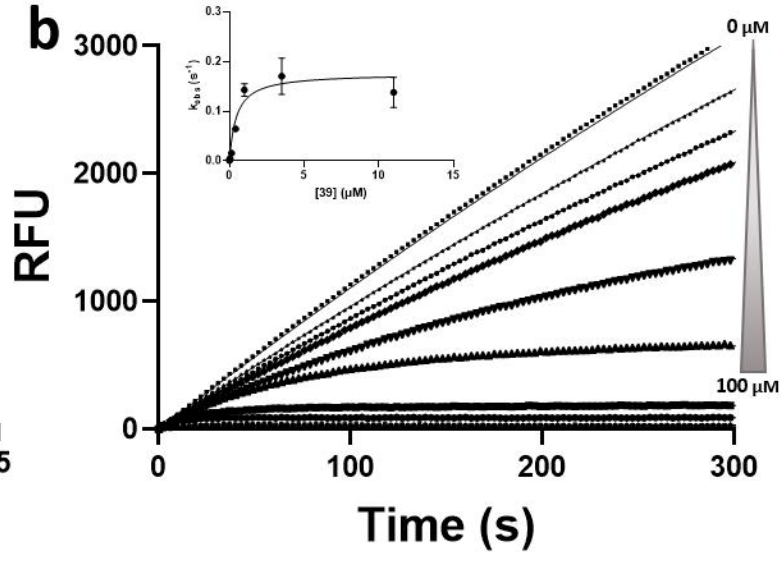


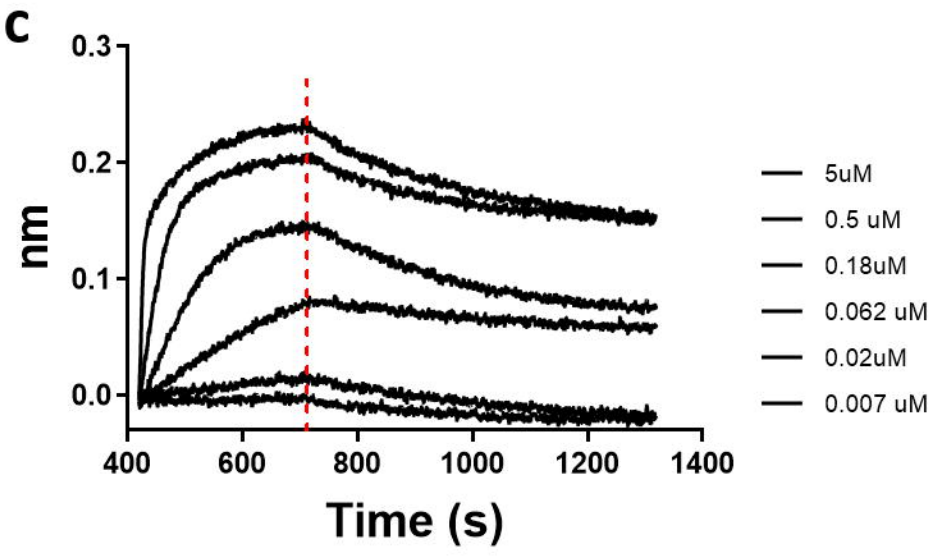


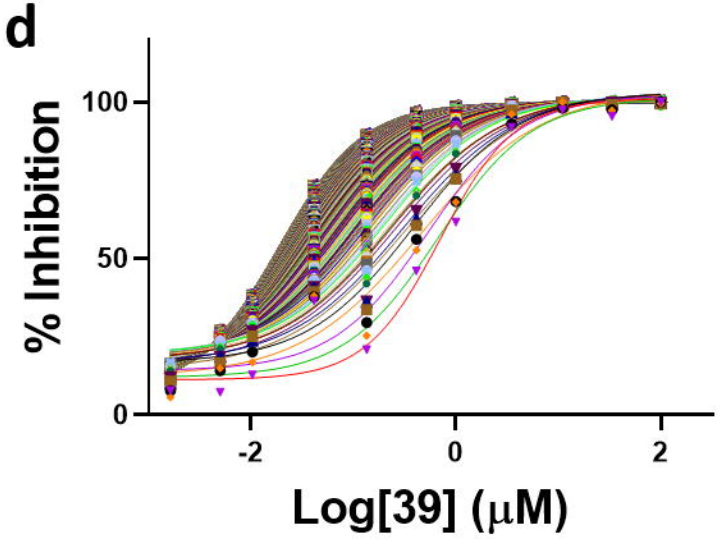


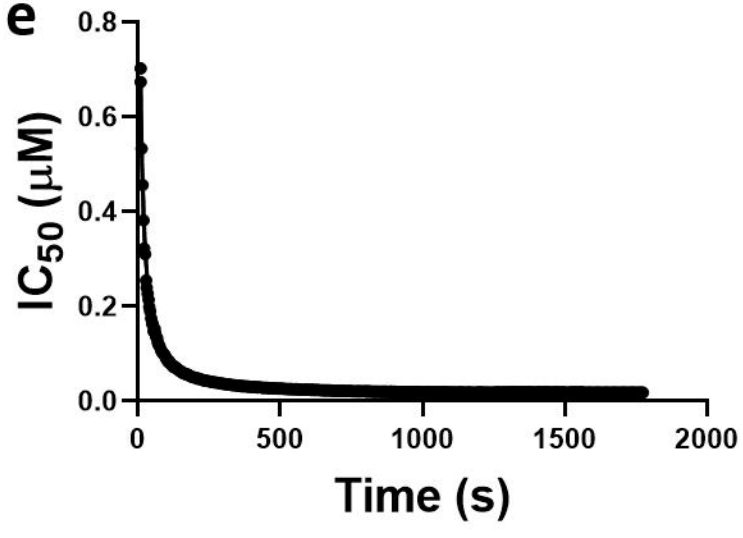


f

| 39 | | |
|---|---|---|
| $IC_{50}$ | (A) | 0.0025 μM |
| $k_{on}$ | (C) | 0.3 $mM^{-1}s^{-1}$ |
| $k_6$ | (B) | 0.00033 $s^{-1}$ |
| $k_5$ | (B) | 0.37 $s^{-1}$ |
| $K_{i(app)}$ | (B) | 1.76 μM |

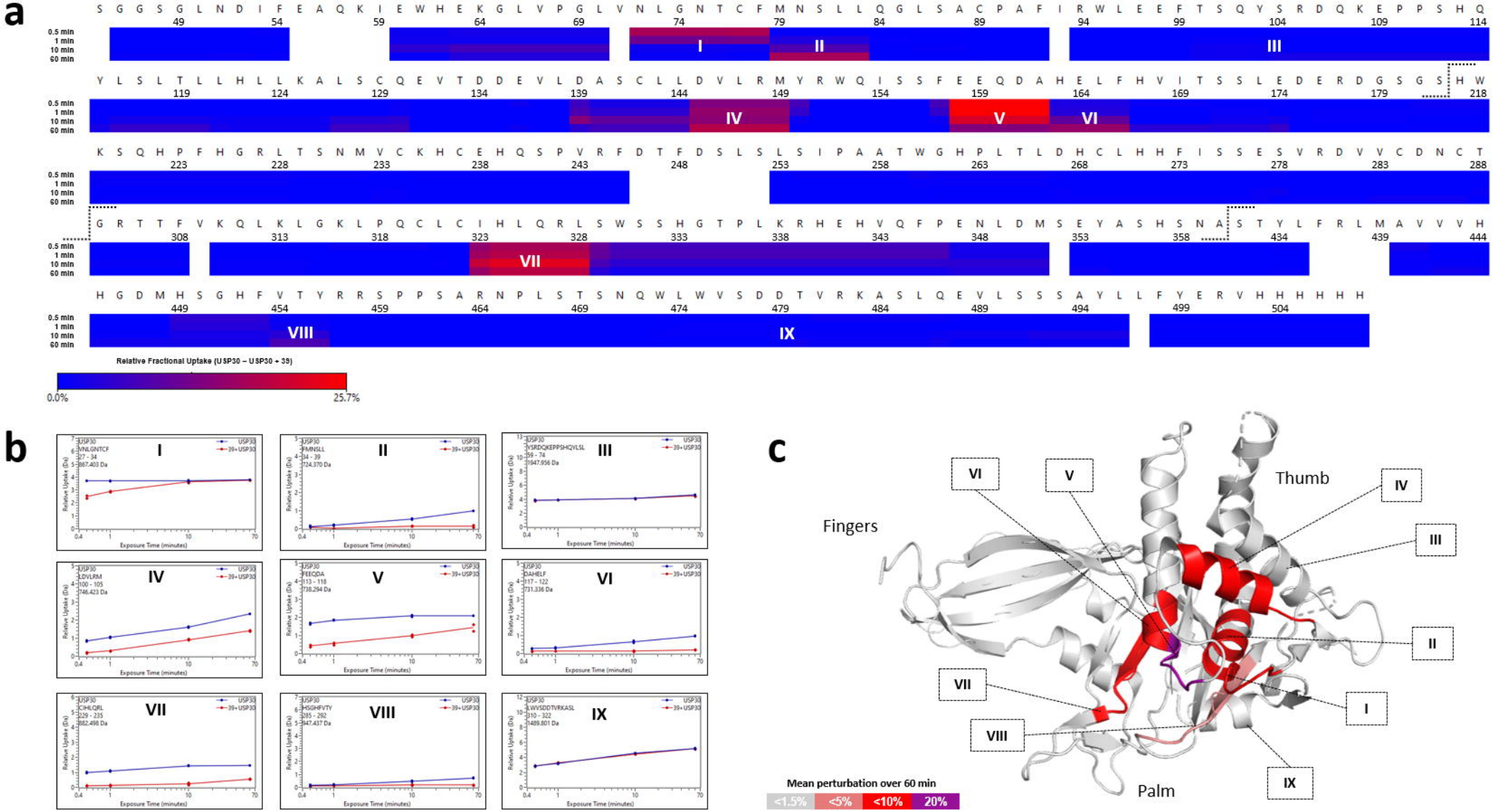
a
0.5 min
1 min
10 min
60 min
I
II
III
IV
V
VI
VII
VIII
IX
Relative Fractional Uptake (USP30 – USP30 + 39)
0.0%
25.7%
b
Exposure Time (minutes)
Relative Uptake (Da)
USP30
39+USP30
c
Fingers
Thumb
Palm
Mean perturbation over 60 min
<1.5%
<5%
<10%
20%

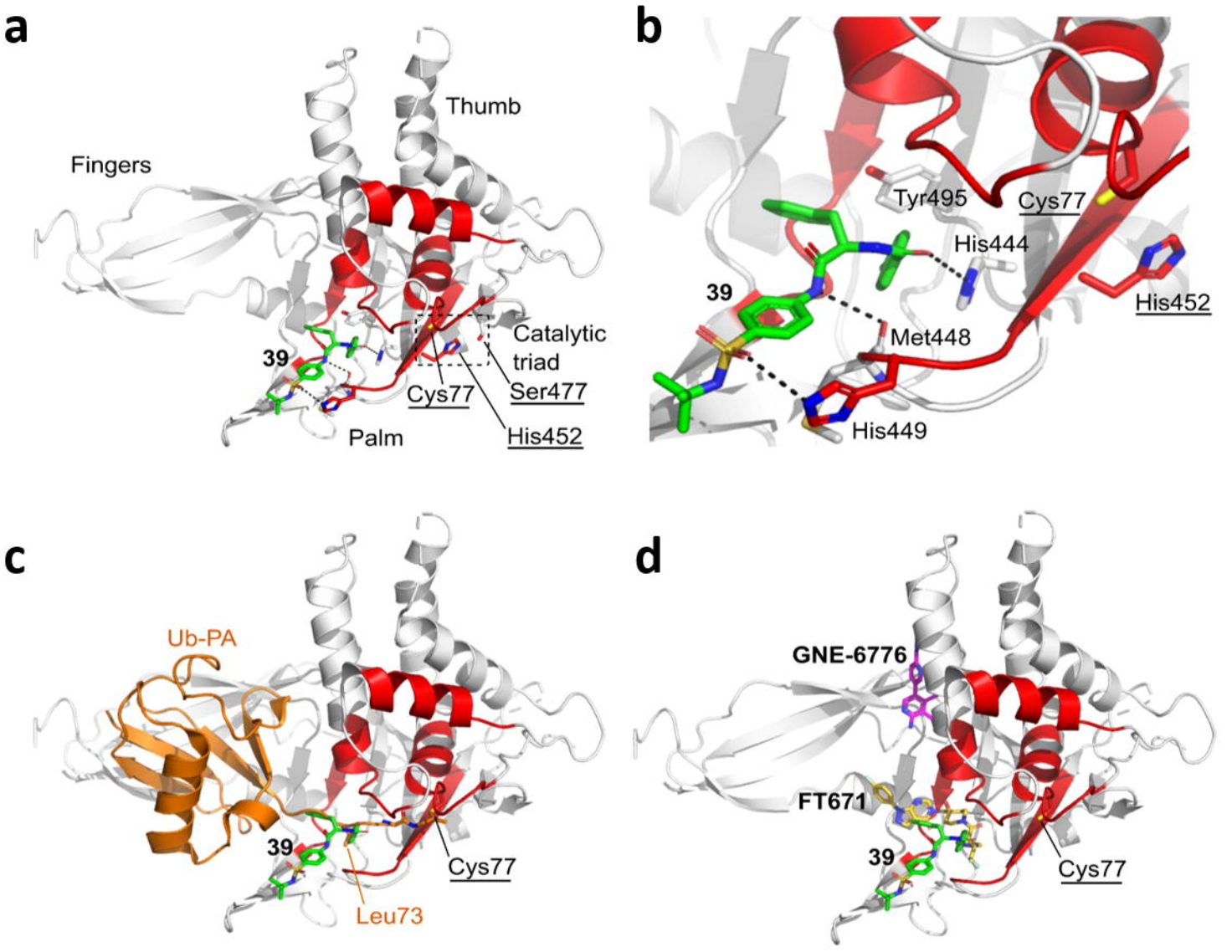
a
Thumb
Fingers
Catalytic
triad
39
Cys77
Ser477
Palm
His452
b
Tyr495
Cys77
His444
39
His452
Met448
His449
c
Ub-PA
39
Cys77
Leu73
d
GNE-6776
FT671
39
Cys77